Improvement of the kinetics of hydrogen release from ammonia borane confined in silica aerogel

Miriam Rueda, Luis Miguel Sanz-Moral, José Juan Segovia, Ángel Martín*
Department of Chemical Engineering and Environmental Technology - University of Valladolid
TERMOCAL Research Group – University of Valladolid

c/ Doctor Mergelina s/n 47011 Valladolid (Spain)
Tel: +34 983423174, e-mail: mamaan@iq.uva.es (Á. Martín)

Improvement of the kinetics of hydrogen release from ammonia borane confined in silica aerogel

Miriam Rueda[1], Luis Miguel Sanz-Moral[1], José Juan Segovia[2], Ángel Martín[1]*

[1]Department of Chemical Engineering and Environmental Technology - University of Valladolid, c/ Doctor Mergelina s/n 47011 Valladolid (Spain)

[2]TERMOCAL Research Group – University of Valladolid, c/ Paseo del Cauce 59 47011 Valladolid (Spain)

Tel: +34 983423174, e-mail: mamaan@iq.uva.es (Á. Martín)

Abstract

Ammonia borane is a promising hydrogen storage material due to its high gravimetric capacity (19.6 % wt), but it also presents limitations such as a slow hydrogen release with a long induction time, a difficult regeneration, or the formation of foams and gaseous by-products during thermolysis. Previous studies have shown that by nanoconfinement of ammonia borane within a porous support some of these limitations can be overcome due to the reduction and stabilization of ammonia borane particle size. However, this effect was only observed with moderate ammonia borane loadings, as with higher loadings the pores of the support became obstructed. In this work, silica aerogels produced by CO_2 drying, with pore volumes up to 2 cm^3/g, have been used to confine ammonia borane. The influence of the amount of ammonia borane loaded on the aerogel support on the thermal and structural properties of the material has been analyzed. It has been found that more than 60 wt% of ammonia borane can be effectively stored in the pores of the aerogel support. The resulting material shows faster hydrogen release kinetics by thermolysis at 80ºC, due to a significant reduction in the mea size of ammonia borane after confinement and the participation of SiOH and SiOSi groups of silica aerogel in the decomposition mechanism.

Keywords: solid state hydrogen storage, ammonia borane, silica aerogel, nanoconfined, supercritical carbon dioxide.

1. Introduction

As fossil fuel reserves are increasingly limited and their use constitute a constant source of greenhouse gases and other environmental problems, the development of alternative energy sources is attracting a considerable attention [1, 2]. In contrast with fossil fuels, which can be easily stored and used when needed, the production of energy from most renewable sources is variable and it cannot be directly controlled. A possible solution for this limitation could be to use hydrogen (H_2) as an energy vector, according to the approach commonly known as 'hydrogen economy' or 'hydrogen society' [3]: Hydrogen can be produced from water (by electrolysis, thermal decomposition, thermochemical processes, photolysis etc.) using renewable energy sources, and stored until needed. Furthermore, the efficiency of the combustion of hydrogen (by combustion in internal combustion engines, catalytic combustion or fuel cells) is high, and it is one of the most environmentally favorable fuels, as it produces nearly zero gaseous emissions.

At large scales, hydrogen can be transported through pipelines (gas H_2) or tankers (liquid H_2), and it is a good energy vector with an energy density of 33 kwh/kg, containing three times more energy than any hydrocarbon fuel on a weight basis [4]. However, the storage of hydrogen in small mobile units such as vehicles or small electronic equipment is more challenging.

These challenges can be quantified analyzing the targets set by the US Department of Energy for 2020 for automotive hydrogen systems: a hydrogen storage gravimetric capacity of 5.5 wt% and a volumetric capacity of 0.040 kg/L, with a maximum cost of 333$/kg H_2 stored [5]. Hydrogen storage by some of most obvious systems using compressed or condensed H_2 cannot fulfill these requirements due to the physical properties of hydrogen. In the former case, high pressures (700 bar to reach a volumetric concentration of 0.042 kg H_2/L) or huge volumes are needed, and in the latter, high energy consumption is unavoidable in order to maintain the required cryogenic temperatures [6]. For these reasons, solid state hydrogen storage materials have been intensively studied, as hydrates [7], metal-organic frameworks [8] or metallic and chemical hydrides [9].

Ammonia borane (AB) is considered as a promising chemical hydride, due to its high hydrogen gravimetric capacity (19.6%wt H_2) and volumetric capacity (140 g/L), moderate decomposition temperature, non-toxicity [10] and stability at room temperature, even in the range 50-60ºC, which is important from the point of view of safety and engineering implications [11]. The thermal decomposition of neat AB releases one mole of hydrogen per mole of AB in each of the following reactions (1), (2) and (3) [12]. In the first decomposition step, AB releases H_2 forming a complex polymeric aminoborane (PAB) below its melting point (114 ºC):

$$BH_3NH_3 \rightarrow BH_2NH_2 + H_2 \qquad T > 120^{\circ}C \qquad (1)$$

Thereafter, PAB decomposes above 120 ºC, forming polymeric iminoborane and small fractions of undesirable volatile byproducts:

$$BH_2NH_2 \rightarrow 1/3\ (BHNH)_3 + H_2 \qquad T > 120^{\circ}C \qquad (2)$$

$$(BHNH) \rightarrow BN + H_2 \qquad T > 500^{\circ}C \qquad (3)$$

Nevertheless, the use of this compound as hydrogen storage material also faces some important limitations. One of them is the kinetic limitation due to the long induction time needed to disrupt the dihydrogen bonding and initiate the release of hydrogen. Furthermore, AB is difficult to regenerate: after thermolysis, it is not possible to restore the initial AB by direct hydrogenation, and complex chemical regeneration routes comprising several steps are needed. Additionally, it forms foams during thermolysis that also complicate the regeneration due to the disruption of the physical structure of the material. Moreover, during the decomposition process, the emission of some volatile byproducts as borazine, diborane or ammonia can be released which could be poisonous for downstream processes and, particularly, hydrogen fuel cells.

Several strategies have been tested to overcome these barriers, including the addition of catalysts as silicon (Si), nickel (Ni), ruthenium (Ru), palladium (Pd) or zinc (Zn) [13-16], confinement of ammonia borane into porous solid supports [17-21], dissolution of AB in ionic liquids [22,23] or using polymers composites [24]. Regarding confinement of AB, different supports have been tested: silica scaffolds as SBA-15 or MCM-48 [18], metal organic frameworks (MOF) [16, 25] or carbon based materials [17] among others. The amount of AB that has been successfully loaded in the support depends on their structural properties (S_{BET} and V_{pores}), getting a maximum amount of 50%wt using silica scaffolds [17]. In all the cases that have been reported, hydrogen kinetic and thermodynamic properties have been improved respect to neat hydride due to the reduction in mean size. In our previous work [26], microparticles of silica aerogel were used as support, getting a maximum concentration of 5%wt AB loaded in hydrophobic silica aerogel. Liquid antisolvent technique was used to precipitate the hydride prior supercritical carbon dioxide drying, resulting in enhanced hydrogen release kinetic compared to pure AB.

In this work, we report the confinement of AB using silica aerogel as porous host. The aerogel has been produced by liquid or supercritical CO_2 drying, a technique that enables to produce a silica material with a high pore volume, and a correspondingly high potential capacity for storage of ammonia borane inside its pores. Several samples with different concentrations of AB up to 60 wt% have been prepared in order to analyze the influence of the loading of AB on the thermal and structural properties of the material. Scanning electron microscopy, N_2 adsorption isotherms, FT-IR spectroscopy and X-ray diffraction have been used in order to characterize the final product prior to the measurement of hydrogen release kinetics by decomposition at 80ºC.

2. Experimental methods

2.1 Materials

Tetramethylorthosilicate (TMOS, 98.0% purity), ammonium hydroxide (NH_4OH, 28.0-30.0% ammonia purity) and ammonia borane (AB, 97% purity) were supplied by Sigma-Aldrich. Figure 1 shows a micrograph of neat AB as received. As shown in this Figure, AB was constituted by agglomerated particles with sizes in the range of 100 μm and with a porous structure. Methanol (MeOH; 99.8% purity), n-hexane (95% purity) and dry tetrahydrofuran (THF; with maximum water of 0.0075wt %) were purchased from Panreac. Carbon dioxide (CO_2, 99.95% purity) was supplied by Carburos Metálicos S.A.

(FIGURE 1)

2.2 Preparation of AB loaded in silica aerogel microparticles

As presented in Figure 2, the procedure for the preparation of AB-loaded silica aerogel microparticles consists of three key steps: preparation of silica gel microparticles, addition of ammonia borane by a wet impregnation method, and drying of the AB-loaded gel particles with pressurized carbon dioxide in order to produce the final, dry AB-loaded aerogel microparticles.

(FIGURE 2)

In the first step of this procedure, hydrophilic silica alcogel was prepared using the well-known method of hydrolysis condensation sol-gel reaction, using TMOS as precursor and methanol as solvent. While with this procedure it is common to prepare large gel monoliths, in this work the gel was synthetized as microparticles, in order to reduce the possible heat and mass transfer resistances that could be caused by larger aerogel monoliths. To do this, and according to the procedure described in a previous work [26], the sol-gel reaction media was dispersed in hexane under mechanical stirring, in order to obtain small droplets of TMOS in methanol dispersed within the hexane continuous phase. After 10 minutes of mechanical stirring of this mixture with a two bladed axial stirrer set at 600 rpm, an aqueous solution of NH_4OH was added as condensation catalyst, which induced the gelation of TMOS. The molar ratio used was the following: 1 mol TMOS: 4.4 mol MeOH: 3.3 mol H_2O: 4.5 mol hexane: 0.08 mol NH_4OH. As methanol or water produced during the condensation reaction can induce the decomposition of ammonia borane during the subsequent drying processes [26], after 2 hours of gelation the alcogel microparticles were retrieved and immersed in THF. Gel particles were then kept during 7 days immersed in THF in a closed vessel, to let the gel age and strengthen its structure. During this ageing period, the THF solvent was renewed at least twice in order to remove the last traces of methanol and water.

After the ageing process, microparticles of alcogel are ready for wet impregnation, adding a solution of ammonia borane dissolved in THF. This method has the advantage that impregnation can be performed under milder temperature conditions compared to melt infiltration, and only one impregnation step is necessary in contrast to incipient impregnation methods [27]. Again, THF was used instead of methanol as solvent in order to avoid methanolysis and therefore the decomposition process of the hydride not only during wet impregnation (due to SiOH groups) but also during drying process [26].

Different samples with different concentrations of ammonia borane were prepared, adding different amounts of hydride (0-0.4g AB dissolved in 5mL of THF) to 2 g of microparticles of alcogel (gel before drying, therefore with the pores filled with the organic solvent) in order to study his influence on the properties of the final solid product. With this, concentrations of AB in the final product ranging from 10 to 60 wt% AB were obtained, where the concentration of AB is defined as presented in equation (4):

$$\%AB = \frac{gAB}{gAB+gaerogel} \tag{4}$$

The third and last step is the removal of the organic solvent in order to obtain the final, dry AB/SiO_2 particles. The drying method employed is a key aspect that determines the textural properties of the porous support. If the solvent is removed by evaporation or lyophilization, the capillary stresses associated to the formation of vapor-liquid interfaces inside the pores of the support cause fractures and a partial collapse of the pore structure of the material. In the case of SiO_2 matrixes, the materials obtained by these drying methods usually show pore volumes below 0.5 – 1.0 cm^3/g. Some examples are the well-known SBA-15 or MCM-41 mesoporous silica matrixes. In contrast, if pressurized or supercritical carbon dioxide is used to extract the solvent, the collapse of the pore structure is minimized, because under these conditions carbon dioxide can be completely miscible with the organic solvent, and therefore the extraction proceeds without formation of gas-liquid interfaces and without capillary stresses. Due to this enhanced preservation of the pore structure, with this method it is possible to reach pore volumes in the range 2 – 4 cm^3/g [28]. Additionally, during this drying process CO_2 can act as antisolvent for solutes dissolved in the organic solvent, as it is completely miscible with the organic solvent, but it cannot dissolve high-molecular weight solutes dissolved in the organic solvent. This precipitation method is commonly referred in the literature as "Gas Anti Solvent" (GAS) or "Supercritical Anti Solvent" (SAS) precipitation [29,30]. In the case of this work, as ammonia borane is insoluble in CO_2 [26], when the THF-immersed alcogels are mixed with CO_2, AB dissolved in the THF that fills the pores of the alcogels quickly precipitates according to a GAS precipitation mechanism, thus favoring the formation of small particles within the pores of the gels.

In a previous work, it was observed that due the interaction of AB with the SiO_2 matrix, the temperature needed to initiate the decomposition of AB is drastically decreased [26]. Thus, in order to avoid the thermolysis of AB, the drying process was carried out at a near-ambient temperature of 25ºC and at a pressure of 100 bar, thus employing pressurized, liquid CO_2. As in the previous work [26], a batch drying apparatus, depicted in Figure 2, was used. Using this apparatus, the alcogels immersed in THF were loaded into the extraction vessel and the system was pressurized with CO_2 using an air-driven piston pump. The system was slowly pressurized at a rate of 0.5 bar/min in order to avoid breakages in the alcogel/aerogel and mechanical stresses that could damage the structural properties of the final product. Once the desired pressure and temperature were reached, the recirculation pump that connects the extraction vessel with the CO_2 reservoir was connected, thus bubbling CO_2 through the THF-immersed alcogels and enhancing the extraction of the solvent. As CO_2 gradually becomes saturated with the solvent during the extraction process, CO_2 in the system was renewed after a predefined extraction time. In this work, four drying cycles were needed (each cycle lasting 60 min, 60 min, 120 min and finally 40 min) to assure the total elimination of organic solvent from the final solid sample. During the CO_2 renewal step after every cycle, the extraction vessel was isolated closing its inlet-outlet valves and kept at the pressure conditions of the drying process to avoid the damages in the structure of the aerogels that could be caused by repeated pressurization-depressurization processes. The rest of the circuit was depressurized till ambient pressure and refilled with the air-driven pump until the extraction pressure of 100 bar. After the last cycle, the entire system was slowly depressurized at a rate of 0.5 bar/min, and samples were retrieved from the extractor and stored until further analysis.

Finally, neat ammonia borane was also recrystallized by GAS process using pressurized CO_2 as antisolvent. These experiments allow evaluating if the recrystallization has a separate, specific influence on the hydrogen release properties of the material. As during aerogel drying AB precipitates inside the pores of the aerogel by a similar mechanism as in these GAS experiments, a similar influence of the recrystallization may be expected that would be combined with the influence of the nanoconfinement within the pores of the aerogel. In these GAS experiments, the same apparatus and experimental procedure previously described for aerogel drying experiments was used, loading the extraction cell with a solution of AB in THF (concentration: 24 mg AB/mL THF).

2.3 Characterization of AB loaded in silica aerogel

2.3.1 Properties of AB/SiO_2

Structural properties were analyzed by Fourier Transform Infrared Spectroscopy (FTIR Bruker, model Alpha with a Platinum-ATR single diffraction sampling module). These analyses were performed before and after dehydrogenation for every concentration of AB loaded in silica aerogel.

The N_2 adsorption-desorption isotherms data were acquired using a Micrometrics Analyzer (ASAP 2020) with N_2 at -196ºC as sorbate. Prior to the analyses, the samples loaded with AB were outgassed under vacuum at room temperature for 2 hours and the silica aerogel without any impregnation compound was degassed under vacuum at 150ºC for several hours (3-5) until the mass of the sample was constant. Total specific surface areas were determined by the multipoint BET method at $P/P_0 = 0.3$, and total specific pore volumes were evaluated from N_2 uptake at $P/P_0 = 0.99$. Pore sizes were calculated using BJH equations.

Scanning electron microscopy (SEM) was performed using a Jeol JSM 820 equipment. Energy Dispersive Microanalysis (EDX) was done with microanalysis Bruker Quantax 2000 at 20Kv obtaining 10000 signals/second. No metallic coating pretreatment was necessary prior to analyses.

X-ray diffraction (XRD) analyses (model Bruker Discover D8) were done at CuKα radiation, λ=1.5418 Å, 2θ angle ranging from 5º to 7º with a scan rate of 4 s/step and a step size of 0.020º. These analyses were also performed before and after thermal dehydrogenation.

2.3.2 Thermal decomposition properties

Thermal gravimetric analyses (TGA) were undertaken in a Mettler Toledo TGA system from 30 to 300ºC at 5ºC/min heating rate under a nitrogen flow rate of 60 mL/min. Differential scanning calorimetry (DSC) assays were carried out in a Mettler Toledo model 822e with a ceramic sensor of high sensitivity. Nitrogen gas flow was also used at 60 mL/min, with the same heating rate (5ºC/min) from 0 to 250ºC using 5-8 mg of sample.

Kinetic measurements of hydrogen release by thermolysis were carried out using a stainless steel cell of 4.7 mL equipped with a certified pressure transducer model DPI104 provided by GE Druck (Germany), which had an uncertainty of ± 0.01 bar and was connected to a data acquisition computer. The cell was loaded with about 100 mg of sample, determining the precise sample weight with an analytical balance with an uncertainty of ± 0.0001 g. Then, the cell was subjected to vacuum, down to an absolute pressure below 0.04 bar. The sample was maintained under vacuum at ambient temperature for at least 30 min, in order to remove small amounts of entrapped gases or moisture that could influence the measurement. Afterwards, the sample was heated to 80ºC introducing the cell inside a chromatographic oven. The pressure evolution in the cell was recorded every 10 seconds using the pressure transducer acquisition software. The amount of hydrogen released was calculated from pressure recordings using the Hydrogen Reference Equation of State [31] implemented in the Reference Fluid Thermodynamic and Transport Properties Database (REFPROP) software developed by the National Institute of Standards and Technology (NIST) [32].

3. Results and discussion

3.1 Incorporation of ammonia borane in silica aerogel

3.1.1 FT-IR studies of neat AB and AB/SiO_2 before thermal decomposition

Figure 3 shows the FT-IR spectra of neat and recrystallized AB [33-35], and of samples with AB-loaded silica aerogel with different concentrations of AB. In the spectra of neat AB, absorption peaks from 3000 to 3500 cm^{-1} can be associated to N-H stretching whereas B-H stretching appears in the range 2000-2500cm^{-1}. Other characteristic peaks in the IR of neat AB appear at 1602 cm^{-1} (N-H deformation), 1372 cm^{-1}(which may be attributed to double B-N bonds [33] or N-H bonds [34]), 1155 cm^{-1} (B-H scissor), 1051 cm^{-1} (N-B-H rock), and N-B bond in the range 720-800 cm^{-1}. As shown in Figure 3, the FT-IR spectrum of recrystallized AB is nearly identical as that of neat AB, indicating that AB has not undergone degradation during the recrystallization.

As presented in Figure 3, the spectrum of silica aerogel shows characteristic peaks at 798 cm^{-1} (Si-O-Si bond), 950cm^{-1} (Si-OH) and 436 cm^{-1} (O-Si-O) [36]. Samples with silica aerogel loaded with AB yield a combination of the characteristic spectra of AB and silica. AB peaks corresponding to B- H bonds near 2000-2500cm^{-1} and N-H bonds near 1600 cm^{-1} are particularly prominent. It can be also observed that, as expected, these peaks show higher intensities in samples with higher proportion of AB. These results indicate that AB is present in samples and has also not undergone degradation during drying of silica aerogel with CO_2.

(FIGURE 3)

3.1.2 Textural properties of AB-loaded silica aerogels

Figure 4 shows the nitrogen adsorption and desorption isotherms of different samples, and Table 1 shows the textural properties obtained from these isotherms. All these isotherms correspond to class IV according to the classification of International Union of Pure and Applied Chemistry (IUPAC), which is typical of mesoporous materials. They show hysteresis due to the capillary condensation, which is observed at higher relative pressure in samples with a higher amount of AB.

(FIGURE 4)

(TABLE 1)

The support obtained in this work shows the typical textural properties of silica aerogels reported in many previous works [37, 38]. Comparing to other mesoporous materials, the surface area of the silica aerogel obtained in this work is similar to that of the Santa Barbara Amorphous (SBA) or MCM silica materials used in previous studies of nanoconfination of AB, but the pore volume is almost twice as high [18, 39], which is a favorable property since this higher pore volume can host a higher concentration of AB.

Moreover, both BET and BJH analyses (see table 1) demonstrate that the surface area and the volume of free pores decrease linearly as concentration of AB increases, variations that correspond well with the amount of AB incorporated into the material [17]. Regarding the BJH distributions of pore volume, the bimodal distribution of the empty support is converted to a unimodal distribution for the sample with highest concentration of AB, as the pores with lower size are filled first with AB, leaving partially empty the biggest ones. In the case of the sample with the highest concentration of AB (60 wt%), only 8% of the pore volume remains free, indicating that this concentration of AB is close to the maximum host capacity of the aerogel. These results suggest that AB was successfully confined inside the pores of the aerogel.

In comparison, in previous works the maximum amount of ammonia borane loaded in SBA or MCM silica supports by a conventional solvent infiltration method was 50 wt% [18, 40], but it was observed that when the concentration of AB was higher than a 33%, it started to aggregate outside the pores of the silica support as the internal pore volume of the material became saturated [25]. In the case of metal organic frameworks (MOF), from 20% wt AB [16] till 50% wt AB [41] has been encapsulated depending on the impregnation method or the MOF used. Also, carbon cryogels have been used as supports employing a wet impregnation method, but achieving a maximum concentration of only 24%wt AB [17] due to the comparatively lower surface area (300 m^2/g) and volume of pores (0.70 g/cm^3) of this support.

3.2 Structural characterization of AB-loaded silica aerogels

3.2.1 Morphology of neat AB, recrystallized AB and AB loaded in silica aerogel

Figure 5-A shows a SEM micrograph of AB recrystallized from THF solutions using pressurized CO_2 as antisolvent. As observed in this figure, the compound is recrystallized as highly agglomerated flat particles. Due to this morphology, it is difficult to obtain precise particle size measurements, but the size estimated by image analysis of SEM micrographs is in the range of 0.5 μm of thickness and 5 μm of length, values that are considerably smaller than the dimensions of neat AB particles as presented in Figure 1. Furthermore, the recrystallized particles do not show the porous, intertwined structure observed in neat AB (Figure 1).

Figure 5-B shows a micrograph of silica aerogel loaded with a 30 wt% of AB. It can be observed that the host silica material is constituted by prismatic particles of 10 – 20 μm, in agreement with the results obtained in a previous work [26]. Furthermore, in SEM micrographs of AB-SiO_2 samples (Figure 5-B), particles with the flat morphology and the dimensions observed in the recrystallized AB (Figure 5-A) are not observed, suggesting that AB did not precipitate as segregated particles outside the aerogel. This impression is confirmed by the results of mapping assays of silica and nitrogen presented in Figure 5. Silica mapping confirms that all the particles that can be observed in the SEM micrograph presented in Figure 5-B indeed correspond to silica aerogel, while nitrogen mapping show that ammonia borane is dispersed within all these particles and is not present as segregated crystals. Therefore it can be concluded that AB is homogenously embedded in the pores of the aerogel. Similar results were obtained in

the mapping of samples with higher concentration of AB, up to the maximum concentration of 60 wt% tested in this work.

(FIGURE 5)

3.2.2 XRD patterns

Figure 6 shows the XRD pattern of neat ammonia borane, which matches well with JCPDS reference 01-074-0894 suggesting the typical polycrystalline structure with tetragonal lattice symmetry, in agreement with literature information about the structure of AB at ambient temperature [42]. The crystallite size estimated using the Scherrer's equation formula is 40 nm, and the dominant sharp peak of the pattern is located at 23.75º, corresponding to (110) planes. After recrystallization by GAS process, slight modifications in the XRD pattern can be observed at $2\theta = 17$ and 30º. A similar modification can be observed in silica-loaded AB samples, although with less defined peaks due to the strong signal produced by the silica support. This modification in the pattern can suggest the formation of diammoniate of diborane (DADB), an isomer of AB. This compound shows some differences regarding the hydrogen release mechanism compared to its isomer AB: the temperature for decomposition of DADB is about 10ºC lower than that of AB, and DADB undergoes solid-phase decomposition without melting or induction period even at moderate temperature, while AB suffers from a long induction period prior to H_2 release [43]. Therefore, the formation of this compound may justify some of the observed thermal properties, as it will be discussed in the following sections.

Nevertheless, in GAS recrystallized samples, the dominant pattern is equivalent to that of neat AB, also corresponding to tetragonal crystal structure is observed, although diffraction peaks are not so well defined, and the estimated crystallite size increases to

75 – 150 nm. In the case of AB loaded in silica aerogel, the peaks are merged, therefore suggesting a reduction of crystallinity or an increased inhomogeneity in the properties of the crystals due to the incorporation in the pores [44]. Additionally, as shown in Figure 5b it can be seen that the XRD pattern of amorphous silica, characterized by a broad peak around 24º, is overlaid to the dominant peaks related to AB. Therefore results show that AB retains its crystalline structure after nanoconfination within the pores of the aerogel, with estimated crystallite sizes in the range 100 – 200 nm, similar to those obtained by recrystallization of AB by GAS process.

(FIGURE 6)

3.3 Thermal characterization of AB-loaded silica aerogels

Figure 7 shows the differential scanning calorimetry (DSC) traces of neat and recrystallized AB compared to samples in which the hydride is loaded in silica aerogel. In the case of the curve of neat AB, a sharp endothermic peak is observed whose onset temperature (T_{on}=108.5 ºC) and peak temperature (T_p=110.8ºC) is dramatically reduced when AB is loaded in silica aerogel (see table 2). This first peak is associated to the melting point [14] or the dissociation of the intermolecular hydrogen bonding [18]. The reduction or elimination in this first peak suggests that the degree of hydrogen bond in the samples in which AB is embedded in silica aerogel is decreased, favoring the reduction of the induction time. A similar result has been observed when AB was embedded in other silica supports [18]. Regarding recrystallized AB, DSC results also show reduction in the onset and peak endothermic temperatures, maintaining the shape of the curve of neat AB. In this case, variations in characteristic temperatures of the DSC traces can be associated to the reduction in the mean particle size achieved by recrystallization of AB. As described by Varin et al [45], a reduction of particle size into the subicrometric or nanometric scale is generally associated to a reduction of the onset and peak temperatures of hydrogen evolution thermal events, due to the destabilization of the material induced by the increased particle surface. Additionally, the reduction of onset temperatures and induction time can be associated to the formation of DADB by recrystallization suggested by XRD assays.

Similar results have been obtained in other works where AB is confined in different supports. In the case of SBA and MCM silica supports, reductions in the onset and peak temperatures to 48ºC and 100ºC have been reported [18], but as previously described lower temperatures have been obtained in this work. This fact can be due to the higher volume of pores of aerogel support that avoids the agglomeration of AB in meso-channels. Therefore higher contact between the particle and the surface of the silica aerogel takes place, enhancing the influence of silica surface groups on the decomposition mechanism. In experiments with MOFs [42] or carbon cryogels [17, 20] as supports, similar modifications in the thermal response of the material have been reported. However, Srinivas et al. [16] observed a reduction of 30ºC in the onset and peak temperatures of decomposition using MOFs, whereas in our case a displacement of almost 70ºC is obtained.

Moreover, DSC results indicate a reduction of the exothermic enthalpy associated with hydrogen release as the proportion silica/AB is increased. The measured enthalpy of reaction for H_2 release from neat AB is -24.9 kJ/mol AB, which is in good agreement with results reported in literature. However, when the proportion silica/AB is increased, the corresponding enthalpy of reaction changes to -10.9 kJ/mol AB for the sample with 60% of AB, and -5.5 kJ/mol AB for the sample with 30% of AB. A reduction of the enthalpy of reaction for H_2 release from AB was also observed by Gutowska et al. [40] in their studies of incorporation of AB in mesoporous SBA-15 silica scaffold. However, these authors report a more drastic variation of the enthalpy to -1.0 kJ/mol AB. These authors indicate that the reason for the reduced exothermicity is the suppression of the formation of boron compounds as byproducts of the PAB that is the main decomposition product of AB according to reaction 1, which had the favorable consequence of reducing the production of gaseous byproducts.

(TABLE 2)

(FIGURE 7)

This hypothesis agrees well with the results obtained in this work by TGA assays. Figure 8 shows the results of TGA analysis performed on neat AB and AB-loaded silica aerogel. In the case of neat AB, two important weight loss steps, which correspond to the decomposition of the hydride, are observed: the first one till 129ºC corresponds to a weight loss of 12.7 wt% and the second one, which finishes at 213ºC, corresponds to a weight loss of 27.5 wt%. In comparison, and in agreement with the results of DSC assays, TGA analysis shows that the AB confined in silica aerogel initiates its decomposition at lower temperatures. It is also noticeable that in this case, weight loss is not confined to sharp steps at defined temperatures, but it proceeds continuously over the temperature range studied. In particular, at temperatures above 200ºC, where as previously discussed neat AB does not experience any additional weight losses, a continuous weight loss is still observed in the case of AB confined in aerogel. This result indicates that the third step of the thermal decomposition mechanism, indicated in reaction (3), also begins at lower temperatures in the case of confined AB compared to neat AB. Moreover, as shown in Table 2, in both cases the total weight loss per unit mass of AB in the sample is significantly larger than the maximum amount of hydrogen that can stored in the compound. Similar results have been reported in [18], suggesting that when AB is heated to high temperatures above 200ºC, other gases apart from hydrogen are produced, as borazine, diborane, ammonia, etc. However, analyzing the results reported in Table 2, it is noticeable that the total amount of volatile compounds produced by heating up to 300ºC is reduced when AB is confined in silica aerogel. This result, together with the variations in DSC assays of confined AB presented before, suggest that interactions between AB and the silica support are taking place that influence the decomposition mechanism of AB. Such interactions were suggested to happen between AB and hydroxyl groups from the silica surface of the host by Lai et al. [18]. These groups can interact with the BH_3 group, loosening the covalent bond between BH_3 and NH_3 groups of AB, thus destabilizing and promoting the decomposition of the compound. Furthermore, by this interaction BH_3 is kept bound to the scaffold reducing the production of borazine and precluding the formation of poliiminoborane

(FIGURE 8)

In figure 9, FTIR of neat AB and AB loaded in silica aerogel is shown before and after dehydrogenation at 80ºC. It is observed that most of the peaks at frequencies related to N-H and B-H bonds are broadened, shifted and decreased of intensity which indicates the disruption of the bonds due to the release of hydrogen [13] in both samples. The same behavior is observed for all the concentrations of AB loaded in silica aerogel, although it is more pronounced at higher concentrations of AB. B-N band in the range 700-900 cm^{-1}, which is observed in all the samples, is weakened but is still detected after dehydrogenation; this fact clarifies that B-N is not disrupted and ammonia formation is avoided during the decomposition [14]. On the other hand, in the sample in which AB is loaded, the bonds related to silica are present without any change after thermal treatment due to its stability at these conditions.

(FIGURE 9)

Regarding the crystallinity of the samples after thermal dehydrogenation, figure 10 shows XRD analyses of byproduct after isothermal dehydrogenation at 80ºC. According to ICDD 00-019-0418, 2θ= 20.1º, 23.6º and 41.1º are assigned to amorphous PAB $(NH_2BH_2)_5$ [46]. In the case of AB/SiO_2 samples, amorphous silica peak is present apart from amorphous PAB byproduct.

(FIGURE 10)

3.4 Kinetics of hydrogen release by thermolysis at 80ºC

Figure 11 shows the kinetics of hydrogen release by thermolysis at 80ºC of neat AB compared with AB confinement in silica aerogel. Results in this figure are normalized reporting the amount of hydrogen released by unit mass of AB in the sample. Due to the design of the cell used to measure kinetics, it was not possible to analyze samples of the gas evolved during themolysis. However, it is assumed that at this temperature, the gas which is released is H_2 [12, 19, 41, 47] and no other volatile gases are present in the gas stream in neat AB nor confined in silica aerogel. Regarding the shape of the curve in neat AB, it follows a sigmoidal kinetic, typical of nucleation and growth pathway, with a long induction time of more than 2 h, as reported in previous works [48]. After confinement in silica, the induction time is reduced significantly. This means that the silica could act as a catalyst (SiOH groups) [40] creating defect sites in the support that initiate the decomposition at lower temperature. On the other hand, at lower concentration of AB in the solution (prior to the drying), the hydride could precipitate in the pores of the silica with lower mean size as was also suggested with XRD analyses and corroborated in BET results. This suggests that smaller particles have more contact with the surface of the silica and an easier way to form different bonds between the two free pair of electrons of O in the Lewis base of Si-O-Si or Si-OH bond from the silica with BH_3 or NH_3 from AB. As result, the intermolecular hydrogen bond is reduced, following the mechanism proposed by Lai et al. [18].

In the case of neat AB, 2 hours are needed to start releasing H_2, and more than 4 hours to get half of its content in H_2 at this temperature ($0.025gH_2/gAB$) whereas only it takes 22 minutes in the case of 13%AB loaded in silica aerogel. This fact shows the improvement of silica aerogel as support for this chemical hydride system.

Regarding to recrystallized sample, it can be observed that the release profile maintains the sigmoidal shape characteristic of neat AB, with a slower hydrogen release than samples loaded in silica aerogel during the first 30 min of thermolysis. However, compared with neat AB, with the particle size reduction achieved by GAS recrystallization the induction time is drastically reduced and the release of hydrogen is accelerated, to the point that after one hour an equivalent amount of hydrogen is released from GAS-recrystallized AB as from AB loaded silica aerogel with a 30 wt% of AB.

(FIGURE 11)

As a complement to Figure 11, Table 3 presents the total hydrogen release per unit mass of solid product (AB + silica aerogel support). Results in this table clearly indicate the weight penalty caused by the use of silica aerogel as porous host, as this material does not contribute to the hydrogen storage capacity, thus reducing the total gravimetric capacity of the material [27]. However, it can be seen that this disadvantage is counterbalanced by a faster hydrogen release during the first 1-2 h of thermolysis.

(TABLE 3)

Moreover, there is a significant visual change in the morphology of neat AB in contrast to AB encapsulated in silica aerogel. Figure 12 shows the different result of AB after thermal decomposition at 80ºC. In the case of neat AB, foaming process takes place at the same time that H_2 is released from the hydride. Thus, even if the material was micronized before thermolysis, this morphology and its associated advantages are completely lost during the thermolysis and therefore in possible future hydrogen cycles, if the material is regenerated [49]. However, when AB is encapsulated in silica aerogel, this process is avoided obtaining particles with the same physical appearance. To confirm this observation, Figure 13 presents SEM/EDX micrographs of the 60%AB/SiO_2 sample after thermolysis. As shown in this figure, the original morphology of the material is preserved after the thermolysis. Furthermore, as indicated by the results of nitrogen mapping, the decomposition products of AB remain homogeneously dispersed within the SiO_2 aerogel matrix. Therefore it can be concluded that by incorporation of AB inside the aerogel the morphological variations of the material due to foaming are avoided.

(FIGURE 12)

(FIGURE 13)

4. Conclusions

Ammonia Borane has been recrystallized and nanoconfined inside the pores of silica aerogel by a novel process, based on a simultaneous aerogel drying and ammonia borane gas antisolvent precipitation using compressed carbon dioxide. Due to the favorable textural properties of the aerogel materials obtained with this method, it has been possible to load aerogels with up to 60 wt% of ammonia borane, without blocking of pores and with a homogeneous dispersion of ammonia borane within the aerogel. By analysis of the thermolysis process, it has been observed that by nanoconfinement the temperature required to initiate the thermolysis process is reduced and the release kinetics are accelerated as they do not show induction time. Furthermore, by nanoconfination of AB, the morphological properties of the material are stabilized and foaming is eliminated, which could be favorable properties for a subsequent material regeneration process. The feasibility of implementation of the multi-step chemical process required to re-hydrogenate AB when this compound is embedded in the silica matrix remains to be tested.

Supplementary Information

Video 1: Thermolysis of neat ammonia borane at 80ºC. Time is accelerated by a factor of 64.

Video 2: Thermolysis of 60%AB/SiO_2 sample at 80ºC. Time is accelerated by a factor of 64.

Acknowledgements

This research has been financed by the Spanish Ministry of Economy and Competitiveness through project ENE2011-24547. Á. Martín thanks the Spanish Ministry of Economy and Competitiveness for a *Ramón y Cajal* research fellowship. M. Rueda thanks the University of Valladolid for a *FPI* predoctoral grant. L. M. Sanz thanks the Spanish Ministry of Economy and Competitiveness for a *FPI* predoctoral grant.

References

[1] M.Balat, Int. J. Hydrogen Energ. 33 (2008) 4013-4029

[2] M.Hook, X.Tang, Energ. Policy 52 (2013) 797-809

[3] S. A. Sherif, F. Barbir, T. N. Veziroglu, Electricity J. 18 (2005) 62-76

[4] J. Graetz, Chem. Soc. Rev. 38 (2009) 73-82

[5] DOE: US Department of Energy. Web site: http://www.doe.gov.

[6] L. O. Williams, D. E. Spond, Appl. Energ. 6 (1980) 99-112.

[7] H. P. Veluswamy, R. Kumar, P. Linga, Appl. Energ.122 (2014) 112-132.

[8] M. Paik Suh, H. J. Park, T. K. Prasad, D. Lim, Chem. Rev. 112 (2012) 782-835

[9] B.Sakintuna, F.Lamari-Darkrim, M.Hirscher, Int. J. Hydrogen Energ. 32 (2007) 1121-1140

[10] B. Peng, J. Chen, Energ. Environ. Sci. 1 (2008) 479-483

[11] S. D. Rassat, C. L. Aardahl, T. Autrey, R. S. Smith, Energ. Fuel. 24 (2010) 2596-2606

[12] G. Wolf, J. Baumann, F. Baitalow, F. P. Hoffmann, Thermochim. Acta 343 (2000) 19-25

[13] D. Kumar, H. A. Mangalvedekar, S. K. Mahajan, Mater. Renew. Sustain. Energy 3 (2014) 23

[14] A. C. Gangal, P. Kale, R. Edla, J. Manna, P. Sharma, Int. J. Hydrogen Energ. 37 (2012) 6741-6748

[15] B. Roy, J. Manna, P. Sharma, J. Alloy Compd. 645 (2015) S234-S238.

[16] G. Srinivas, J. Ford, W. Zhou, T. Yildirim, Int. J. Hydrogen Energ. 37 (2012) 3633-3638

[17] A. Feaver, S. Sepehri, P. Shamberger, A. Stowe, T. Autrey, G. Cao, J. Phys. Chem. B 111, (2007) 7469-7472

[18] S-W Lai, H-L. Lin, T.L.Yu, L-P. Lee, B-J. Weng, Int. J. Hydrogen Energ. 37 (2012) 14393-14404

[19] T.Autrey, A.Gutowska, L.Li, J.Linehan, M.Gutowski, Preprints of Papers-American Chemical Society, Division of Fuel Chemistry 49 (2004) 150-151

[20] S.Sepehri, B.B.Garcia, G.Cao, J. Mater. Chem. 18 (2008) 4034-

[21] S.Sepehri, A.Feaver, W.J.Shaw, C.J.Howard, Q.Zhang, T.Autrey, G.Cao, J. Phys. Chem. B 111 (2007) 14285-14289

[22] R.K.Ahluwalia, J.K.Peng, T.Q.Hua, Int. J. Hydrogen Energ. 36 (2011) 15689-15697

[23] M. J. Valero-Pedraza, A. Martín-Cortés, A. Navarrete, M. D. Bermejo, Á. Martín. Kinetics of hydrogen release from dissolutions of ammonia borane in different ionic liquids. Energy 91 (2015) 742-750.

[24] S.F.Li, Z.W.Tang, Y.B.Tan, X.B.Yu, J. Phys. Chem. C 116 (2012) 1544-1549

[25] L-Q Wang, A.Karkamkar, T.Autrey, G.J.Exarhos, J. Phys. Chem. C 113 (2009) 6485-6490

[26] M.Rueda, L.M.Sanz-Moral, A. Nieto-Márquez, P.Longone, F.Mattea, A.Martín, J. Supercrit. Fluids 92 (2014) 299-310

[27] T. Nielsen, F.Besenbacher, T.R.Jensen, Nanoscale 3, (2011) 2086-2098

[28] A.S. Dorcheh, M. H. Abbasi., J. Mater. Process. Tech. 199 (2008) 10-26

[29] E. Reverchon, R.Adami, G.Caputo, I. de Marco, J. Supercrit. Fluids 47 (2008) 70-84

[30] M.Rueda, L.M Sanz-Moral, A.Martín, Cryst. Growth Des. 14 (2014) 4768-4776

[31]J. W. Leachman, R. T. Jacobsen, S. G. Penoncello, E. W. Lemmon, J. Phys. Chem. Ref. Data 38 (2009) 721-748.

[32] E. W. Lemmon, M. L. Huber, M. O. McLinden. NIST Standard Reference Database 23: Reference Fluid Thermodynamic and Transport Properties-REFPROP, Version 9.1, National Institute of Standards and Technology, Standard Reference Data Program, Gaithersburg, 2013.

[33] M.R.Weismiller, S.Q.Wang, A.Chowdhury, S.T.Thynell, R.A.Yetter, Thermochim. Acta 551 (2013) 110-117

[34] F.Leardini, M.J.Valero-Pedraza, E.Perez_Mayoral, R.Centelli, M.A.Bañares, J. Phys. Chem.C 118 (2014) 17221-17230

[35] J.Smith, K.S.Seshadri, D.White, J. Mol. Spectrosc. 45, (1973) 327-337

[36] R.Al-Oweini, H. El-Rassy, J. Mol. Struct. 919 (2009) 140-145

[37] M.Alnaief, I.Smirnova, J. Supercrit. Fluids 55 (2011) 1118-1123

[38] S.Smitha, P.Shaiesh, P.R.Aravind, S.R.Kumar, Micropor. Mesopor. Mat. 91 (2006) 286-292

[39] W-J Son, J-S Choi, W-S Ahn, Micropor. Mesopor. Mat 113 (2008) 31-40

[40] A.Gutowska, L.Li, Y.Shin, C.M.Wang, X.S.Li, J.C.Linehan, R.S.Smith, B.D.Kay, B.Schmid, W.Shaw, M.Gutowski, T.Autrey, Angewa. Chem. Int. Ed. 44 (2005) 3578-3582

[41] Z.Li, G.Zhu, G.Lu, S.Quiu, X.Yao, J. Am. Chem. Soc. 132 (2010) 1490-1491

[42] A.Paolone, O.Palumbo, P.Rispoli, R.Cantelli, T.Autrey, J. Phys. Chem. C 113 (2009) 5872-5878

[43] Z. Fang, J. Luo, X. Kang, H. Xia, S. Wang, W. Wen., X. Zhou, P. Wang, Phys. Chem. Chem. Phys. 13 (2011) 7508-7513.

[44] H.Kim, A.Karkamkar, T.Autrey, P.Chupas, T.Proffen, J. Am. Chem. Soc. 131 (2009) 13749-13755

[45] R. A. Varin, T. Czujko, Z. S. Wronski. Nanomaterials for Solid State Hydrogen Storage, Springer, New York, 2009.

[46] U.B.Demirci, S.Bernard, R:Chiriac, F.Toche, P.Miele, J. Power Sources 196 (2011) 279-286

[47] F.Baitalow, J.Baumann, G.Wolf, K.Jaenicke-Robler, G.Leitner, Thermochim. Acta 391 (2002) 159-168

[48] A.C.Stowe, W.J.Shaw, J.C.Linehan, B.Schmid, T.Autrey, Phys. Chem. Chem. Phys. 9 (2007) 1831-1836

[49] A.D.Sutton, A.K.Burrel, D.A.Dixon, E.B.Garner, J.C.Gordon, T.Nakagawa, K.C.Ott, J.P.Robinson, M.Vasiliu, Science 331 (2011) 1426-1429

Figure Captions

Figure 1. - SEM micrograph of neat ammonia borane as received

Figure 2. - Steps for preparation of silica aerogel microparticles loaded with ammonia borane.

Figure 3. FTIR spectra of a) silica aerogel b) neat AB c) recrystallized AB d)30%AB/SiO$_2$ e)60%AB/SiO$_2$. Curves are vertically displaced for clarity

Figure 4.-Nitrogen adsorption-desorption isotherms and BJH pore size distribution of silica aerogel and AB loaded in silica with different concentration (●) adsorption (■) desorption

Figure 5.- SEM images of A) Recrystallized AB after recrystallization in THF using liquid CO$_2$ as drying method B) 30%AB loaded in silica aerogel and mapping of sample B (blue is referred to silica and red to Nitrogen)

Figure 6. –a) XRD of neat ammonia borane, recrystallized ammonia borane and AB loaded in silica aerogel with different concentrations b) Amplification of XRD signal showing the characteristic pattern of silica aerogel. Curves are vertically displaced for clarity

Figure 7. - DSC curves of AB and AB loaded in silica aerogel with different concentration. The curves are normalized according to the weight of AB, and vertically displaced for clarity.

Figure 8. - TGA curves of AB and AB loaded in silica aerogel

Figure 9. - FTIR spectra of neat AB and AB loaded in silica aerogel before and after thermolysis dehydrogenation at 80ºC. Curves are vertically displaced for clarity

Figure 10. - XRD of neat AB and AB loaded in silica aerogel after thermolysis

dehydrogenation at 80ºC. * indicates the peaks related to polyaminoborane (PAB) and + refers to amorphous silica peak

Figure 11. - Isothermal kinetic of hydrogen releases from AB and AB loaded in silica aerogel with different concentrations at 80ºC. (The curves are normalized according to the amount of AB in the sample)

Figure 12.- Photographs of neat AB and 60%AB/SiO_2 before and after the isothermal H_2 release by thermolysis at 80ºC a) neat AB before thermolysis, b) neat AB after thermolysis, c) AB/SiO_2 before thermolysis, d) AB-SiO_2 after thermolysis. Video clips of the thermolysis process are provided as Supplementary Information

Figure 13.- SEM image of 60%AB/SiO_2 sample after thermolysis (A), with results of N (B) and Si (C) mapping.

Tables

Table 1.-BET surface areas and BJH pore volumes and pore diameters of silica aerogel dried with liquid or supercritical CO_2 at and AB-loaded silica aerogel

Sample	**BET surface area (m^2 g^{-1})**	**Pore volume (cm^3 g^{-1})**	**Pore diameter (nm)**
SiO_2 sc drying	723.1±2.0	1.35	7.6
SiO_2 Liquid drying	887.3±1.4	1.94	8.7
13AB/SiO_2	216.6±0.3	0.82	11.1
30AB/SiO_2	137.3±0.3	0.56	10.9
60AB/SiO_2	30.4±0.1	0.17	13.7

Table 2. - Temperature data and weight losses of neat and recrystallized AB vs loaded in silica aerogel with different concentration obtained from DSC and TGA analyses respectively.

Sample	**T_{on1} (ºC)**	**T_{p1} (ºC)**	**T_{on2} (ºC)**	**T_{p2} (ºC)**	**Total wt loss per wt AB**
Neat AB	108.5	110.8	113.9	114.1	40.2
Recrystallized AB	70.5	77.9	102.4	113.4	-
60% AB/SiO_2	37.6	62.3	84.8	108.9	33.0
30% AB/SiO_2	39.5	68.7	83.1	99.0	-

Table 3. - Amount of H_2 released at different times by isothermal thermolysis at 80ºC in neat and recrystallized vs. AB loaded in silica aerogel with different concentration

Sample	**15min mgH_2/gtotal**	**30min mgH_2/gtotal**	**45min mgH_2/gtotal**	**1h mgH_2/gtotal**	**2h mgH_2/gtotal**	**final mgH_2/gtotal**
neat AB	0	0	0	0	2	52
AB recrystallized	1,66	7,45	20,19	30,45	43,98	52
13%AB/SiO_2	2,26	4,28	5,28	5,80	6,38	6,76
30%AB/SiO_2	1,69	4,43	7,30	9,07	12,31	14,56
60%AB/SiO_2	2,48	9,42	17,79	20,65	27,27	32,24

Figures

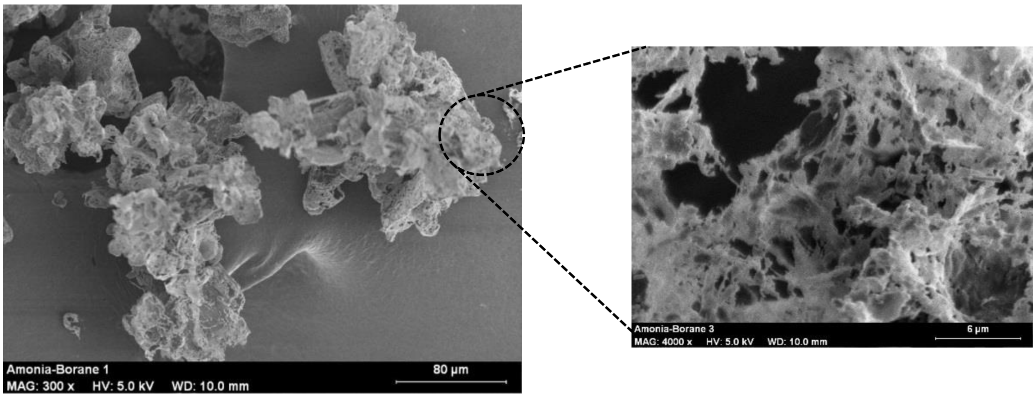

Figure 1. - SEM micrograph of neat ammonia borane as received

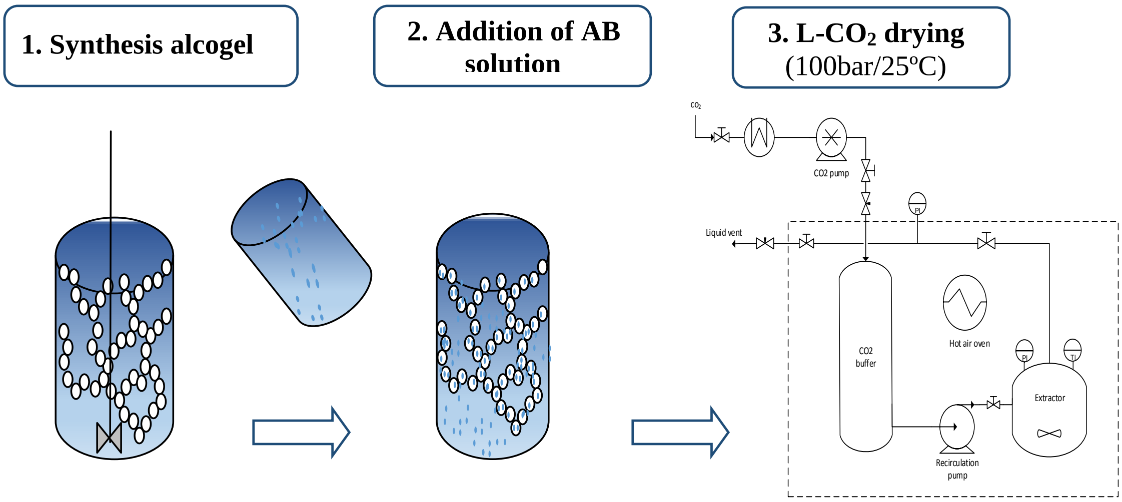

Figure 2. - Steps for preparation of silica aerogel microparticles loaded with ammonia borane.

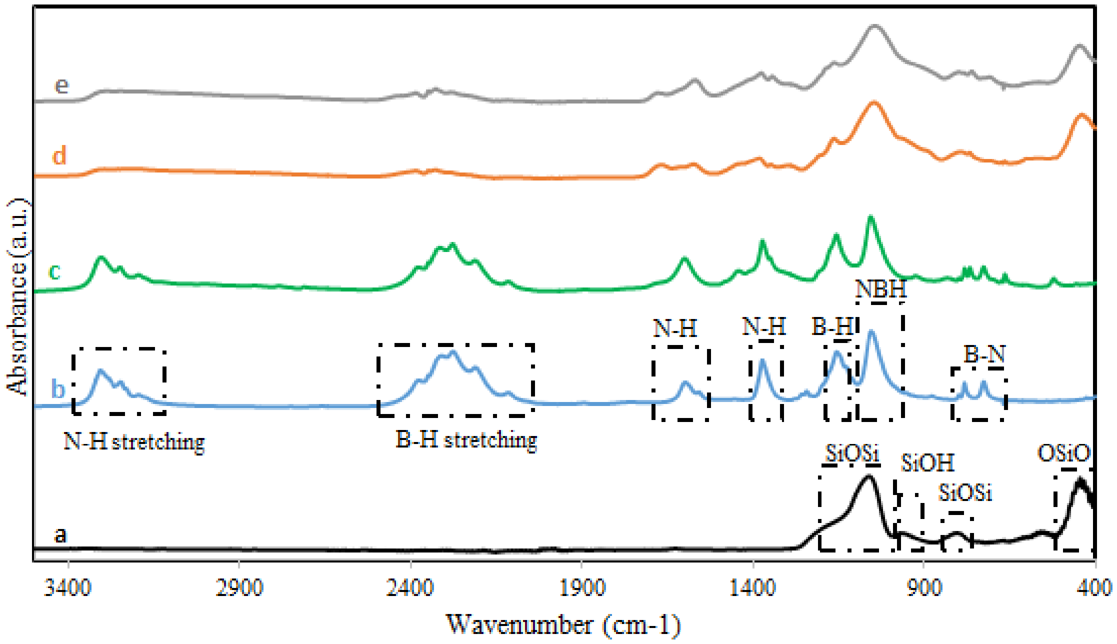

Figure 3. FTIR spectra of a) silica aerogel b) neat AB c) recrystallized AB d)30%AB/SiO_2 e)60%AB/SiO_2. Curves are vertically displaced for clarity.

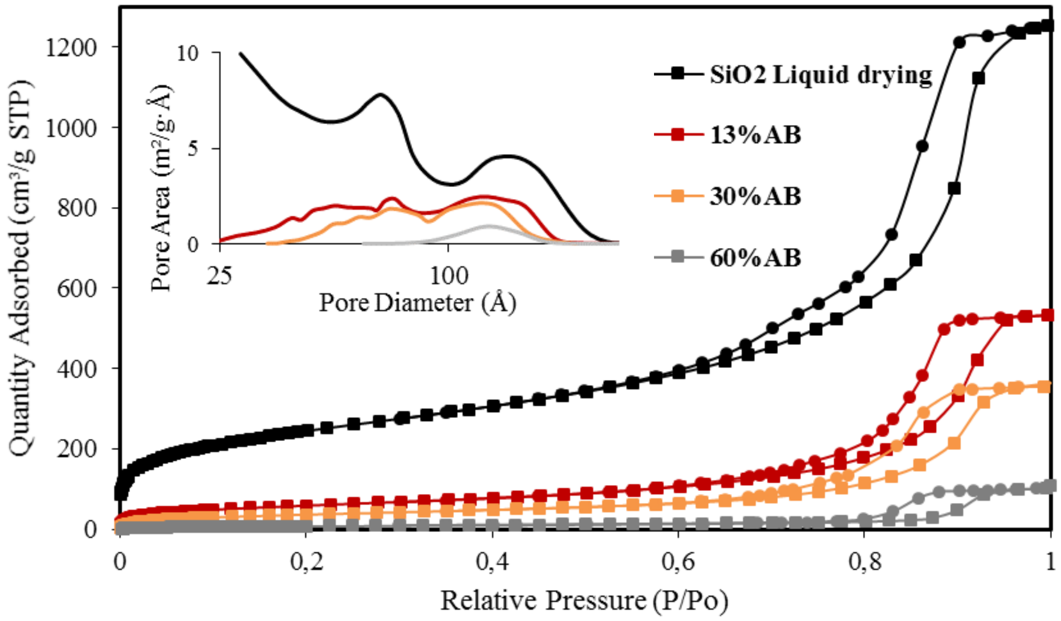

Figure 4.-Nitrogen adsorption-desorption isotherms and BJH pore size distribution of silica aerogel and AB loaded in silica with different concentration (●) adsorption (■) desorption

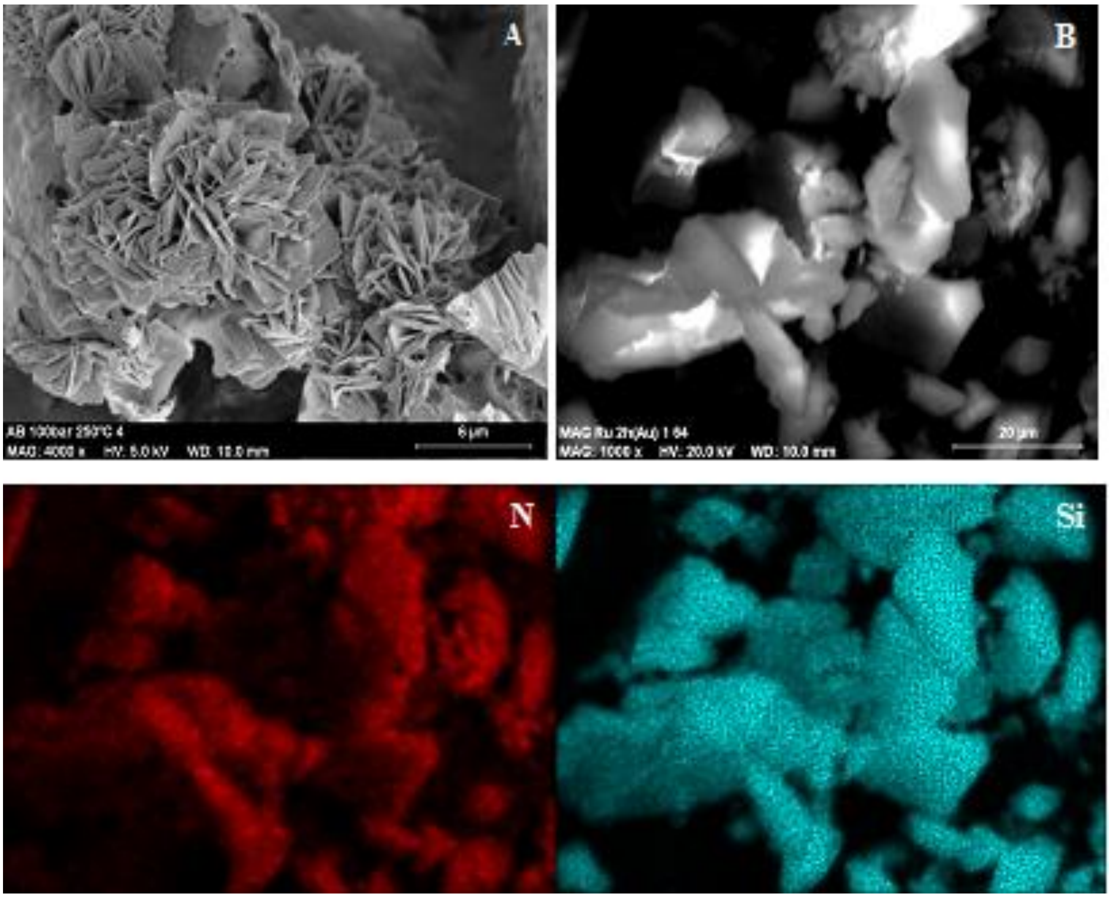

Figure 5.- SEM images of A) Recrystallized AB after recrystallization in THF using liquid CO_2 as drying method B) 30%AB loaded in silica aerogel and mapping of sample B (blue is referred to silica and red to Nitrogen)

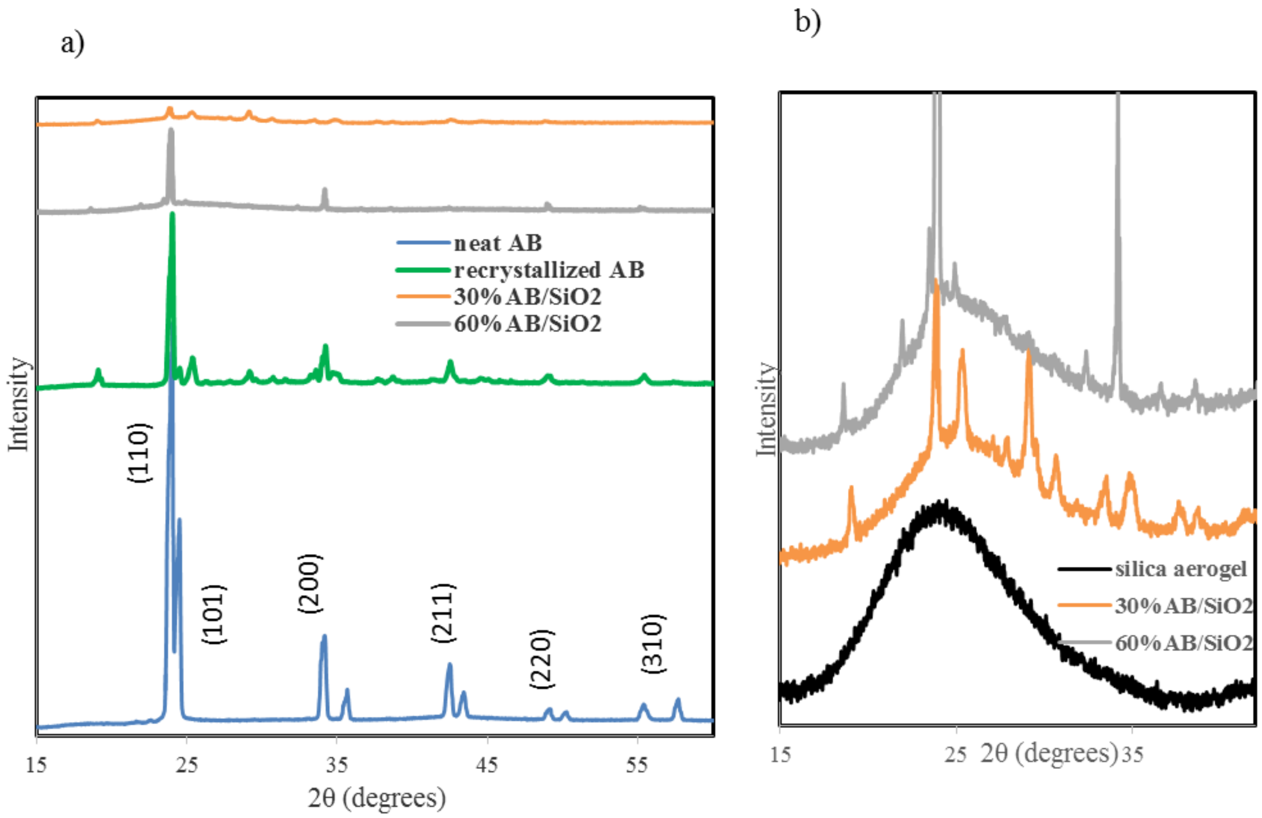

Figure 6. –a) XRD of neat ammonia borane, recrystallized ammonia borane and AB loaded in silica aerogel with different concentrations b) Amplification of XRD signal showing the characteristic pattern of silica aerogel. Curves are vertically displaced for clarity

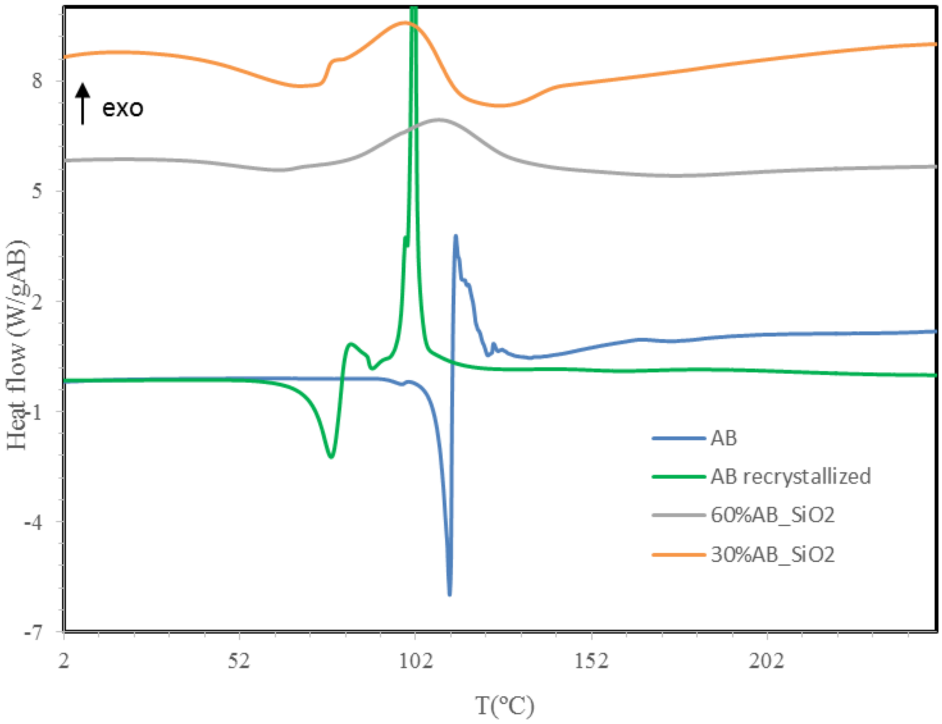

Figure 7. - DSC curves of AB and AB loaded in silica aerogel with different concentration. The curves are normalized according to the weight of AB, and vertically displaced for clarity.

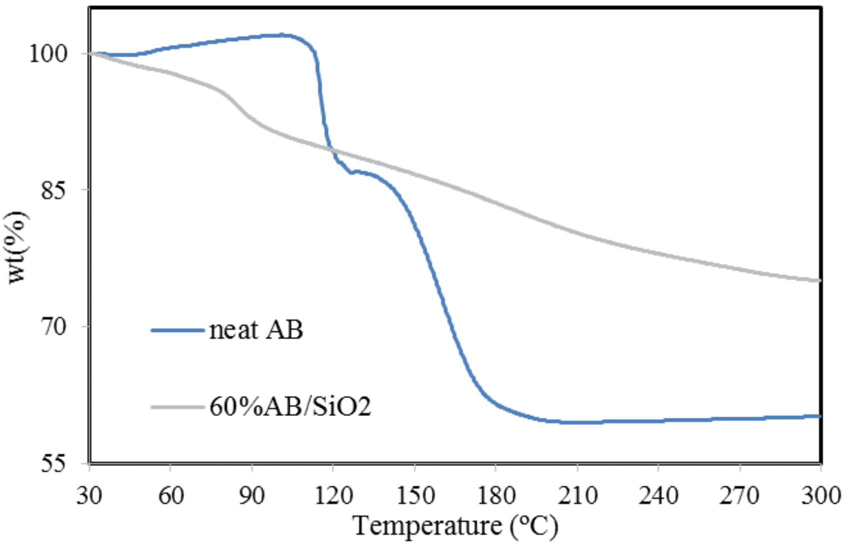

Figure 8. - TGA curves of AB and AB loaded in silica aerogel

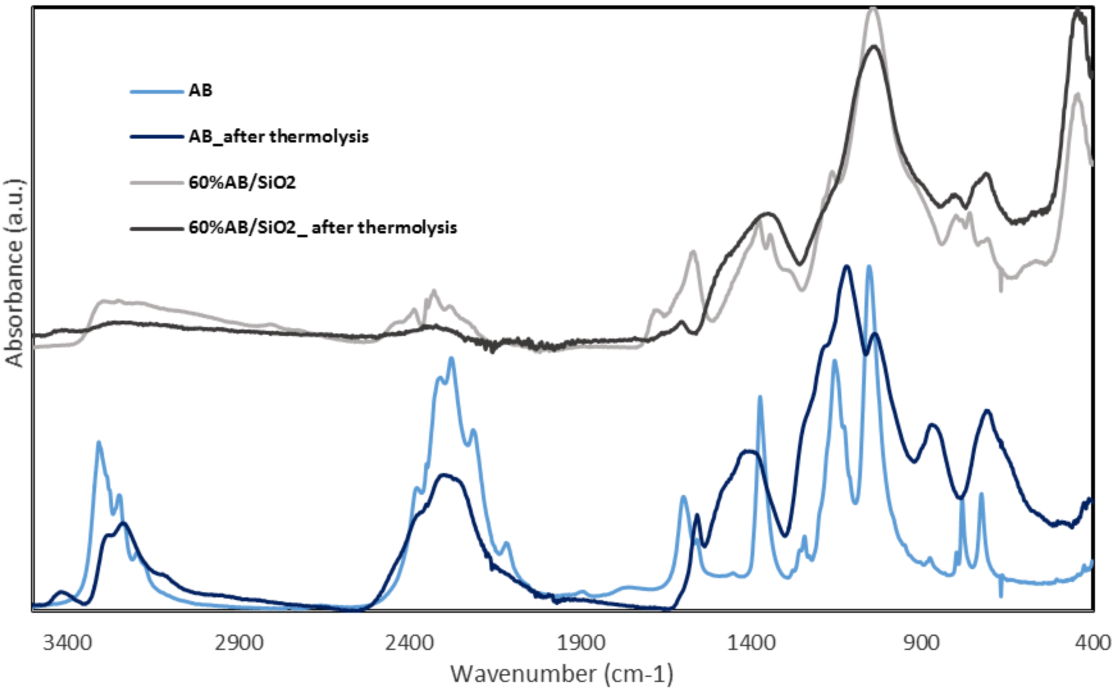

Figure 9. - FTIR spectra of neat AB and AB loaded in silica aerogel before and after thermolysis dehydrogenation at 80ºC. Curves are vertically displaced for clarity

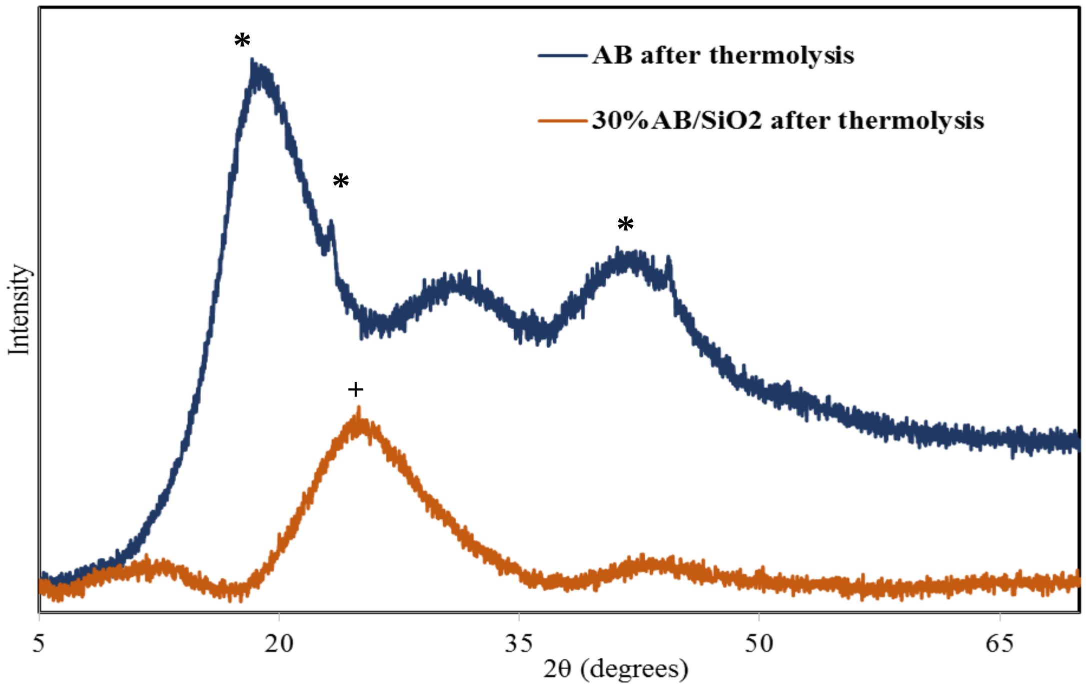

Figure 10. - XRD of neat AB and AB loaded in silica aerogel after thermolysis dehydrogenation at 80ºC. * indicates the peaks related to polyaminoborane (PAB) and + refers to amorphous silica peak

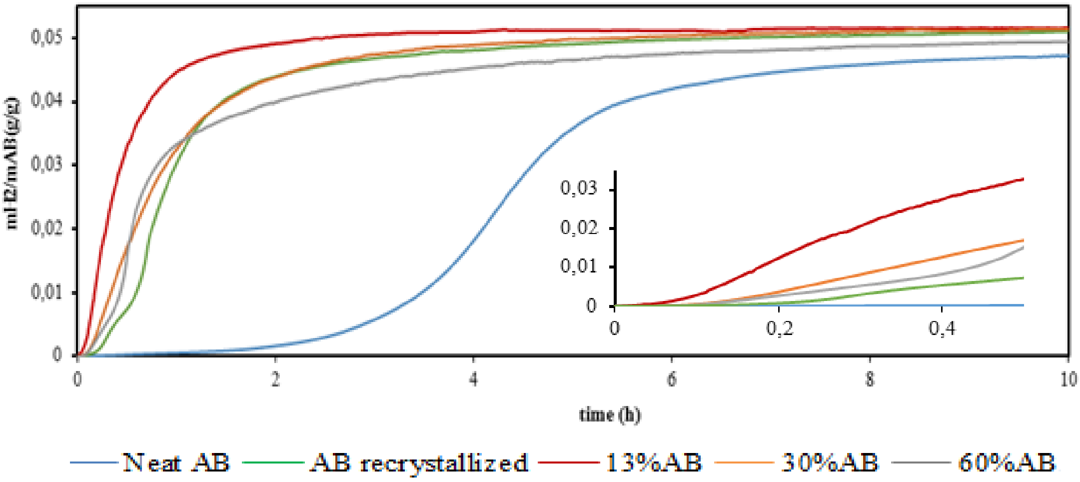

Figure 11. - Isothermal kinetic of hydrogen releases from AB and AB loaded in silica aerogel with different concentrations at 80ºC. (The curves are normalized according to the amount of AB in the sample)

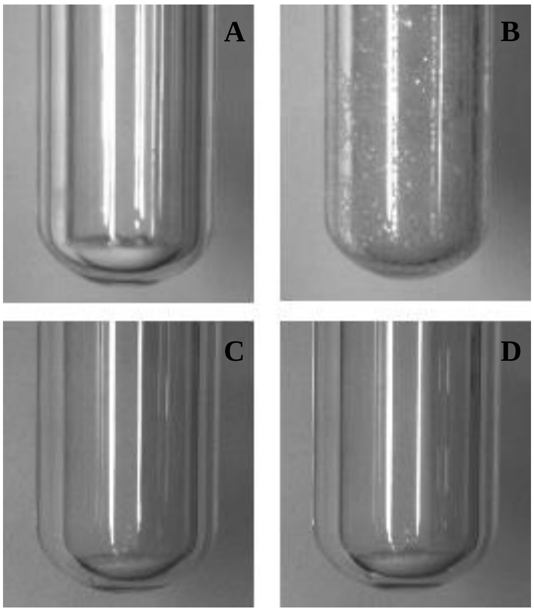

Figure 12.- Photographs of neat AB and 60%AB/SiO_2 before and after the isothermal H_2 release by thermolysis at 80ºC a) neat AB before thermolysis, b) neat AB after thermolysis, c) AB/SiO_2 before thermolysis, d) AB-SiO_2 after thermolysis. Video clips of the thermolysis process are provided as Supplementary Information

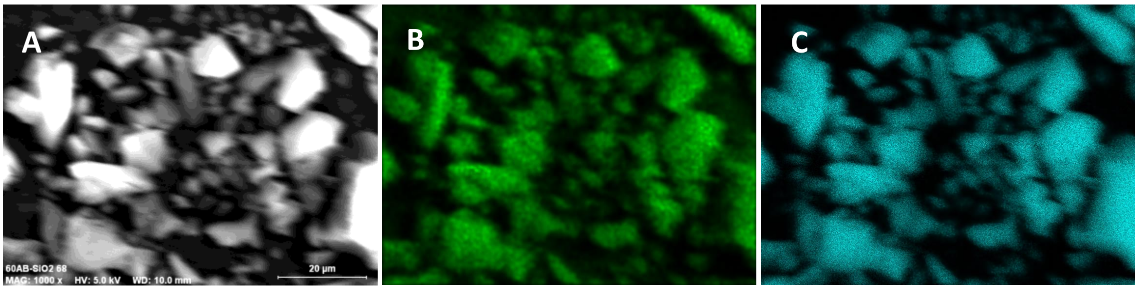

Figure 13.- SEM image of 60%AB/SiO_2 sample after thermolysis (A), with results of N (B) and Si (C) mapping.